AIP Journal of Applied Physics

Effects of lattice mismatch and bulk anisotropy on interband tunneling in broken-gap heterostructures

A. Zakharova, S. T. Yen, K. Nilsson, and K. A. Chao

Citation: Journal of Applied Physics **97**, 063704 (2005); doi: 10.1063/1.1857058
View online: http://dx.doi.org/10.1063/1.1857058
View Table of Contents: http://scitation.aip.org/content/aip/journal/jap/97/6?ver=pdfcov
Published by the AIP Publishing

Articles you may be interested in
Cyclotron resonance study in InAs/AlSb quantum well heterostructures with two occupied electronic subbands
J. Appl. Phys. **111**, 093711 (2012); 10.1063/1.4712042

Band hybridization and spin-splitting in InAs/AlSb/GaSb type II and broken-gap quantum wells
J. Appl. Phys. **108**, 053709 (2010); 10.1063/1.3476059

Valence band effective mass of non- c -plane nitride heterostructures
J. Appl. Phys. **107**, 123105 (2010); 10.1063/1.3448578

Barrier roughness effects in resonant interband tunnel diodes
J. Appl. Phys. **90**, 6177 (2001); 10.1063/1.1415539

Self-consistent modeling of the current–voltage characteristics of resonant tunneling structures with type II heterojunctions
J. Appl. Phys. **82**, 2421 (1997); 10.1063/1.366261

Re-register for Table of Content Alerts

Create a profile.

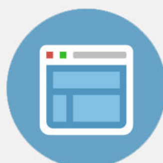

Sign up today!

[This article is copyrighted as indicated in the article. Reuse of AIP content is subject to the terms at: http://scitation.aip.org/termsconditions. Downloaded to] IP: 140.113.38.11 On: Thu, 01 May 2014 03:06:01

HTML ABSTRACT + LINKS

JOURNAL OF APPLIED PHYSICS **97**, 063704 (2005)

Effects of lattice mismatch and bulk anisotropy on interband tunneling in broken-gap heterostructures

A. Zakharova
Institute of Physics and Technology of the Russian Academy of Sciences, Nakhimovskii Avenue 34, Moscow 117218, Russia

S. T. Yen
Department of Electronics Engineering, National Chiao Tung University, Hsinchu, 30050 Taiwan, Republic of China

K. Nilsson[a] and K. A. Chao
Department of Physics, Lund University, Sölvegatan 14A S 223 62 Lund, Sweden

(Received 1 September 2004; accepted 14 December 2004; published online 9 March 2005)

We have studied the effects of bulk anisotropy and the strain induced by lattice mismatch on the interband tunneling in broken-gap single-barrier InAs/AlSb/GaSb heterostructures and double-barrier InAs/AlSb/GaSb/InAs/AlSb/GaSb heterostructures. We have used the eight-band $\mathbf{k}\cdot\mathbf{p}$ model and the scattering matrix method, combined with the Burt envelope function theory, to calculate the interband transmission coefficients through the broken-gap heterostructures. We have found a noticeable anisotropy of the transmission coefficients when the magnitude of the in-plane wave vector increases to around 0.25 nm^{-1}. We have also found that the strain and the bulk anisotropy of quasiparticle dispersion produce additional peaks in the tunneling probability. For the double-barrier resonant-tunneling structures we discover a large spin splitting of the resonant-tunneling peaks caused by the lack of inversion symmetry. A strong influence of the strain induced by lattice mismatch appears in the current–voltage characteristics of the studied broken-gap heterostructures. In InAs/AlSb/GaSb structures the interband tunneling processes into the heavy-hole states contribute mainly to the peak current density if the sample is grown on InAs, but if the sample is grown on GaSb the interband tunneling processes into the light-hole states become the main contribution to the peak current density. As a result, the structure grown on GaSb has a much larger peak current density. This phenomenon was observed experimentally.
© *2005 American Institute of Physics*. [DOI: 10.1063/1.1857058]

I. INTRODUCTION

Interband tunneling structures based on InAs, GaSb, and AlSb materials have been much studied both experimentally and theoretically. In these so-called broken-gap heterostructures, the InAs conduction band overlaps with the GaSb valence band. Consequently, electrons from the InAs conduction band can tunnel into the GaSb valence band through the AlSb barrier layer. This unique band structure makes the broken-gap heterostructures promising candidates for device applications because of their negative differential resistance with high values of peak-to-valley current ratio and peak current density.[1–10] Both single-barrier and double-barrier interband tunneling broken-gap heterostructures have been fabricated and investigated experimentally. Single-barrier structures usually contain an AlSb barrier as a quantum region sandwiched between an n^+-InAs emitter and a p^+-GaSb collector.[2,4,5] In Ref. 3, a similar structure, but with a GaSb/AlSb quantum region, was investigated. Two types of double-barrier structures have been well studied: one is the structure with an AlSb/GaSb/AlSb quantum well[1,11] sandwiched between two InAs cladding layers and the other is that with an AlSb/InAs/AlSb quantum well[7,8] sandwiched between two GaSb cladding layers. In Ref. 9 a complicated double-barrier structure with an AlSb/GaSb/InAs/AlSb quantum well between an n^+-InAs emitter and a p^+-GaSb collector was investigated. It has been shown that these double-barrier structures have higher peak-to-valley current ratios than the single-barrier structures.

Theoretical analysis on interband tunneling processes in broken-gap heterostructures should consider the mixing of the states in conduction band (CB), light-hole (LH) band, and heavy-hole (HH) band, with or without the split-off (SO) hole band. The existing theoretical works use the tight-binding method,[11–13] or the multiband $\mathbf{k}\cdot\mathbf{p}$ quantum transmitted boundary method,[14] or the transfer-matrix method,[15,16] or the transfer Hamiltonian approach.[17,18] While the interband tunneling of electrons from the CB states into the LH states has been proven to be the dominating process in general, the tunneling into the HH states cannot be ignored for oblique incidence. For example, the interband tunneling processes through the HH states in the InAs/AlSb/GaSb resonant-tunneling structure (RTS) contribute considerably to the valley current density.[11,12,17]

The lattice mismatch in broken-gap heterostructures is small, and its effect is usually neglected. The strain-induced energy shift in InAs/GaSb broken-gap quantum wells was investigated very recently.[19] Based on these results, we ex-

[a]Electronic mail: karin.nilsson@teorfys.lu.se

[This article is copyrighted as indicated in the article. Reuse of AIP content is subject to the terms at: http://scitation.aip.org/termsconditions. Downloaded to] IP: 140.113.38.11 On: Thu, 01 May 2014 03:06:01

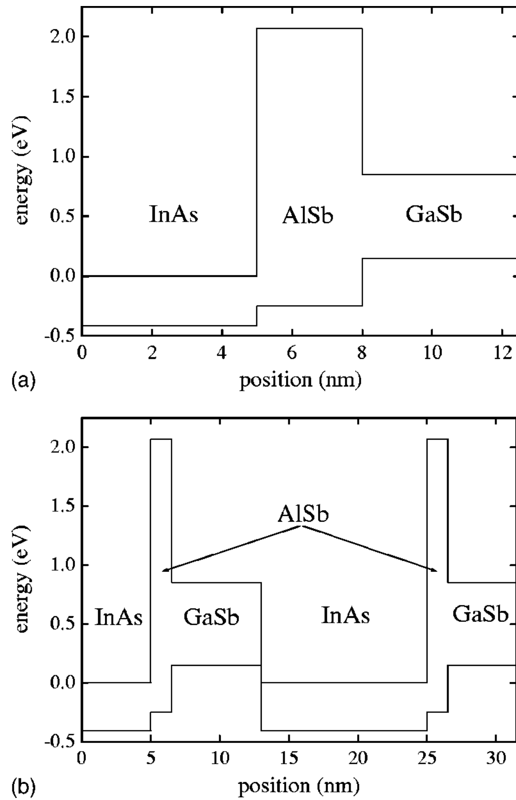

FIG. 1. The energy band diagrams of (a) the InAs/AlSb/GaSb single-barrier structure and (b) the InAs/AlSb/GaSb/InAs/AlSb/GaSb resonant-tunneling structure.

pect that the small energy-level shift in the quantum well due to the lattice mismatch is important for resonant tunneling, because this small level shift may easily destroy the resonant-tunneling condition. The effect of lattice mismatch manifests itself for oblique incidence owing to the complicated two-dimensional dispersion parallel to interfaces. In the present work, we will extend our previous study of the static properties of broken-gap quantum wells to the investigation of the effects on dynamical interband tunneling properties of tunneling heterostructures not only of the strain but also of the bulk anisotropy. In particular, we will demonstrate these effects on the transmission coefficients and the current–voltage ($I-V$) characteristics. We will use the scattering matrix method[20] and the relevant eight-band $\mathbf{k}\cdot\mathbf{p}$ model.[19] In our analysis we will also use the Burt envelope function theory[21] and its extension to the heterostructures of zinc-blende materials.[22] The interband transmission coefficients for carriers with a finite magnitude of the in-plane wave vector along the [10] and [11] directions are calculated.

The systems we have investigated are an InAs/AlSb/GaSb single-barrier structure, as shown in Fig. 1(a), grown on either InAs or GaSb substrates, and an InAs/AlSb/GaSb/InAs/AlSb/GaSb resonant-tunneling double-barrier structure grown on GaSb, as indicated in Fig. 1(b). Due to the lattice mismatch, for an InAs/AlSb/GaSb structure grown on InAs, the AlSb layer and the GaSb layer are strained, and for an InAs/AlSb/GaSb structure grown on GaSb, the AlSb layer and the InAs layer are strained. When the InAs layer is strained, the conduction-band edge shifts downwards by 0.029 eV. When the GaSb layer is strained, the edge of the heavy-hole band shifts upwards by 0.019 eV, and the edge of the light-hole band shifts downwards by 0.029 eV. Consequently, these two single-barrier structures will have different electron energy-level structures. For the double-barrier structure, the strain induced by the lattice mismatch also changes the subband dispersion in the InAs/GaSb quantum well.[19,23] Combined with the modification of the bulk dispersion due to bulk anisotropy, the transmission coefficients and the $I-V$ characteristics of broken-gap heterostructures will then exhibit interesting behavior which will be studied in the present work.

We have found a noticeable anisotropy of the transmission coefficients when the in-plane wave vectors have a magnitude around 0.25 nm^{-1}. Under various situations, the bulk anisotropy produces additional peaks in the interband tunneling probability into the LH states. On the other hand, the strain induced by lattice mismatch creates additional peaks in interband tunneling probability into the HH states in the spectrum region where tunneling into LH states is forbidden. For the single-barrier structures, we obtained a larger tunneling current density for the sample grown on GaSb than on InAs, in agreement with the experiment.[4,5] For the double-barrier heterostructures, we obtained a large spin splitting of the peaks in the transmission coefficients. However, the complicated multiple-peak profile of the transmission coefficients results in one broad maximum in the $I-V$ characteristics.

In Sec. II we will outline our model and method of calculation of the electron transmission coefficients and the tunneling current density. A detailed numerical calculation will then be performed, and the numerical results will be discussed in Sec. III. Finally, a conclusion is given in Sec. IV.

II. MODEL AND METHOD OF CALCULATION

In the present work, we will consider two strained tunneling heterostructures grown along the crystallographic [001] direction, which defines the z axis. We also assign the [100] direction as the x axis and [010] the y axis. The two tunneling heterostructures are InAs/AlSb/GaSb and InAs/AlSb/GaSb/InAs/AlSb/GaSb, and under flatband conditions without strain their band diagrams are shown in Fig. 1 as panels (a) and (b), respectively. We will use the $\mathbf{k}\cdot\mathbf{p}$ band model which takes into account the CB states, the LH states, the HH states, and the SO hole states. It was pointed out[19] that the effect of the following terms are small: the linear-in-k terms and Kane's B parameter in the $\mathbf{k}\cdot\mathbf{p}$ Hamiltonian, the terms proportional to the interband deformation potential caused by the lack of inversion symmetry in bulk zinc-blende crystals, and the spin-orbit terms in the strain Hamiltonian. So, these terms will be neglected in our theoretical analysis. The resulting Hamiltonian of the eight-band model around the Γ point of zinc-blende crystals can be written as

$$\hat{H} = \hat{H}_k + \hat{H}_{\mathrm{SO}} + \hat{H}_{\epsilon}, \tag{1}$$

where the terms $\hat{H}_{\mathrm{SO}}$ and $\hat{H}_{\epsilon}$ describe the spin-orbit interaction and the effect of strain, respectively. The term $\hat{H}_k$ depends on the conduction-band edge, the valence-band edge,

[This article is copyrighted as indicated in the article. Reuse of AIP content is subject to the terms at: http://scitation.aip.org/termsconditions. Downloaded to] IP: 140.113.38.11 On: Thu, 01 May 2014 03:06:01

the momentum operators $\hbar\hat{k}_x$, $\hbar\hat{k}_y$, and $\hbar\hat{k}_z$, the modified Luttinger parameters, as well as the interband momentum matrix elements. The exact forms of the 8×8 matrices $\hat{H}_k$, $\hat{H}_{SO}$, and $\hat{H}_\epsilon$, as well as the basis functions for the Hamiltonian are given in Ref. 19. The multicomponent envelope function $\boldsymbol{\psi}=(\psi_1,\psi_2,\psi_3,\psi_4,\psi_5,\psi_6,\psi_7,\psi_8)^T$ and the corresponding eigenenergy E satisfy the equation $\hat{H}\boldsymbol{\psi}=E\boldsymbol{\psi}$. Unphysical solutions of this equation are removed with a standard procedure.[19,22] After this, the boundary conditions for the envelope functions are derived.[19]

To solve the equation for $\boldsymbol{\psi}$ with the scattering matrix method, we divide the entire system into N sublayers and in each sublayer the potential is approximated by a constant value. The envelope functions in each sublayer are then expressed as linear combinations of the corresponding bulk eigenstates whose wave vectors are permitted to have an imaginary part. Let z_{n1} and z_{n2} mark the positions of the two interfaces at the left and right sides of the nth layer, respectively. In the nth sublayer, there are plane-wave-like functions with the z-component wave vectors $\pm k_{z,j}^{(n)}$ for the jth bulk eigenstate. Consequently, in the nth sublayer the envelope function $\boldsymbol{\psi}_n$ can be written in the form

$$\boldsymbol{\psi}_n = e^{i(k_x x+k_y y)}\sum_{j=1}^{6}\left[a_j^{(n)}e^{ik_{z,j}^{(n)}(z-z_{n1})}\mathbf{f}_{+j}^{(n)} + b_j^{(n)}e^{-ik_{z,j}^{(n)}(z-z_{n2})}\mathbf{f}_{-j}^{(n)}\right], \tag{2}$$

where the complex wave vectors $k_{z,j}^{(n)}$ have non-negative imaginary parts. The coefficients $a_j^{(n)}$ and $b_j^{(n)}$ are for the forward and backward waves, respectively. The column vectors $\mathbf{f}_{\pm j}^{(n)}$ and the complex wave vectors $k_{z,j}^{(n)}$ satisfy the equation $\hat{H}[k_x,k_y,\pm k_{z,j}^{(n)}]\mathbf{f}_{\pm j}^{(n)}=E\mathbf{f}_{\pm j}^{(n)}$. We choose mutually orthogonal vectors $\mathbf{f}_{\pm j}^{(n)}$ corresponding to each of the wave vectors $\pm k_{z,j}^{(n)}$.

When we solve the Schrödinger equation for each sublayer of the structure, we use the boundary conditions to construct the 12×12 scattering matrix $S(1,N)$ which connects the coefficients of the initial layer 1 and the final layer N, as in Ref. 19. Here, layer 1 is the left cladding layer and layer N is the right cladding layer. If the electron tunnels from state l of the left cladding layer to the right side of the structure, then $\mathbf{b}^{(N)}=0$, $a_l^{(1)}=1$, and $a_j^{(1)}=0$ for $j\neq l$, where state l must be a propagating state with a real $k_{z,l}^{(1)}$. The vectors $\mathbf{a}^{(N)}$ and $\mathbf{b}^{(1)}$ are determined from

$$\mathbf{a}^{(N)} = S_{11}(1,N)\mathbf{a}^{(1)}, \tag{3}$$

and

$$\mathbf{b}^{(1)} = S_{21}(1,N)\mathbf{a}^{(1)}, \tag{4}$$

where the 6×6 submatrices $S_{11}(1,N)$ and $S_{21}(1,N)$ can be obtained from the scattering matrix $S(1,N)$ and are defined in Ref. 19.

To calculate the transmission of electrons along the z axis, from the left cladding layer to the right cladding layer, let us first consider the corresponding velocity operator,

$$\hat{v}_z = \frac{i}{\hbar}(\hat{H}z - z\hat{H}) = \frac{1}{\hbar}\frac{\partial\hat{H}}{\partial\hat{k}_z}. \tag{5}$$

Replacing the operator $\hat{k}_z$ in $\hat{v}_z$ by $k_{z,l}^{(n)}$, we obtain the 8×8 matrix representation $J_{z,l}^{(n)}$ for the probability current-density operator, which is equal to the velocity operator, in the nth sublayer corresponding to the lth state with a real $k_{z,l}^{(n)}$. For the left cladding layer ($n=1$), the incident probability current density is then calculated as

$$j_{z,l}^{(1)} = |a_l^{(1)}|^2\mathrm{Re}[\mathbf{f}_l^{(1)\dagger}J_{z,l}^{(1)}\mathbf{f}_l^{(1)}] = \mathrm{Re}[\mathbf{f}_l^{(1)\dagger}J_{z,l}^{(1)}\mathbf{f}_l^{(1)}]. \tag{6}$$

Using the scattering matrix method, the transmitted probability current density for the tunneling process into the kth state of the right cladding layer ($n=N$) is simply

$$\begin{aligned} j_{z,k}^{(N)} &= |a_k^{(N)}|^2\mathrm{Re}[\mathbf{f}_k^{(N)\dagger}J_{z,k}^{(N)}\mathbf{f}_k^{(N)}] \\ &= |[S_{11}(1,N)]_{kl}|^2\mathrm{Re}[\mathbf{f}_k^{(N)\dagger}J_{z,k}^{(N)}\mathbf{f}_k^{(N)}]. \end{aligned} \tag{7}$$

In terms of these two probability current densities, the tunneling probability T_{kl} from the lth state of the left cladding layer into the kth state of the right cladding layer is obtained as

$$T_{kl}(E,\mathbf{k}_\parallel) = j_{z,k}^{(N)}/j_{z,l}^{(1)}. \tag{8}$$

It is important to notice that if $k_{z,l}^{(1)}$ [or $k_{z,k}^{(N)}$] has a nonzero imaginary part, then the corresponding wave is incapable of propagating and the respective probability current density $j_{z,l}^{(1)}$ [or $j_{z,k}^{(N)}$] vanishes.

The tunneling probability also depends on the applied bias voltage V which modifies the potential profile of the entire system. Under this condition and with the consideration of the carrier occupations of the initial and final states, the partial current density $I_{kl}(V)$ for the interband tunneling processes from the incident state l into the transmitted state k can be calculated as

$$\begin{aligned} I_{kl}(V) = \frac{e}{4\pi^2\hbar}\int dk_\parallel k_\parallel \int dE T_{kl}(E,k_\parallel,V) \\ \times[f_1(E,\mu_1) - f_2(E,\mu_2)], \end{aligned} \tag{9}$$

where e is the electronic charge. The functions $f_1(E,\mu_1)$ and $f_2(E,\mu_2)$ are the Fermi–Dirac distribution functions for the left InAs cladding layer and the right GaSb cladding layer, with the corresponding chemical potentials μ_1 and μ_2. We have neglected the variation of the chemical potential in each cladding layer caused by the drift-diffusion processes. The total current density is simply the sum of all the partial ones.

We treat electrons and holes classically in the cladding layers, as in Ref. 17. The good agreement between the calculated and measured $I-V$ curves given in Ref. 17 suggests that this approximation is reasonable. The values of μ_1 and μ_2 with respect to the conduction-band edge of the left cladding layer near the quantum region, as well as the potential profile, are derived by solving the Poisson equation throughout the entire heterostructure but neglecting the charge accumulation in the quantum region. This approximation is excellent for the single-barrier structures. However, it is also reasonable for the resonant-tunneling structures considered here with sufficiently thin InAs and GaSb layers in the quan-

[This article is copyrighted as indicated in the article. Reuse of AIP content is subject to the terms at: http://scitation.aip.org/termsconditions. Downloaded to] IP: 140.113.38.11 On: Thu, 01 May 2014 03:06:01

tum well, where the difference between the highest hole level and the lowest electron level is not large. We also found that the effect of anisotropy of the transmission coefficients on the total current density is negligibly small. Therefore, in our numerical results this effect is ignored.

III. RESULTS AND DISCUSSION

The systems to be studied here are single-barrier and double-barrier tunneling structures, the band diagrams of which, under flatband condition, are plotted in the two panels of Fig. 1. We need many material parameters as input to our numerical calculation. In Ref. 24 we can find the values of the energy gaps, the split-off energies, the interband momentum matrix elements, the Luttinger parameters, the lattice constants, and the band offsets for both the conduction band and the valence band. The deformation potentials and the stiffness constants are given in Ref. 25. While the numerical analysis is performed, attention is paid to the following issue. The strain due to the lattice mismatch distorts both the conduction- and the valence-band edges from the flatband situation given in Fig. 1, resulting in a change of the bulk dispersion, as well as the subband dispersion in the InAs/GaSb quantum well.[19,23] Adding the effect of bulk anisotropy which also modifies the bulk dispersion, interesting phenomena are expected to be found in both the transmission coefficients and the $I-V$ characteristics.

A. Single-barrier structures

For the single-barrier InAs/AlSb/GaSb structure we have studied, the electron tunnels from a state in the InAs conduction band, through the AlSb barrier layer, into either a LH state or a HH state in the GaSb valence band. Two types of InAs/AlSb/GaSb heterostructures were investigated experimentally: one grown on InAs (Ref. 5) and the other on GaSb.[4] We will study both structures with the barrier width of 3 nm. The electron from the InAs emitter tunnels through the AlSb barrier layer near its LH and HH valence-band edges. Hence, it can transfer through the AlSb layer both as the LH states and HH states for nonzero in-plane wave vector, but not as the SO hole states, the wave functions of which vanish inside the barrier because the SO band edge is far away from the energies of the tunneling electrons. The LH effective mass is much less than the HH effective mass. For this reason the depth of wave-function penetration into the barrier is much less for the HH state than for the LH state, and therefore the tunneling process through the LH channel dominates. In the structure grown on InAs, the LH band edge of the barrier layer shifts by −0.054 eV due to the lattice-mismatched strain, while it shifts only by −0.027 eV in the structure grown on GaSb. For this reason the depth of LH state penetration into the barrier for a given incident electron energy E is lesser for the structure grown on InAs than for the structure grown on GaSb. Hence, the interband tunneling probability is expected to be larger in the second case.

If an incident electron has zero in-plane wave vector, $\mathbf{k}_{\parallel}=0$, it can only tunnel into the LH valence band of the GaSb contact layer. Hence, we will consider the more interesting case of finite $\mathbf{k}_{\parallel}$ for which the electron can tunnel into both the LH and the HH states. The calculated transmission coefficients for $\mathbf{k}_{\parallel}=0.09\ \mathrm{nm}^{-1}$ along the [10] direction are shown in Fig. 2 with the solid curves for tunneling into all HH states of different spin orientations (CB-HH tunneling) and the dashed curves for tunneling into all LH states (CB-LH tunneling). Panel (a) is for the unstrained InAs/AlSb/GaSb structure. The results for strained structures grown on InAs and on GaSb are plotted in panels (b) and (c), respectively. The results for $\mathbf{k}_{\parallel}$ in the [11] direction differ only slightly from those shown in Fig. 2.

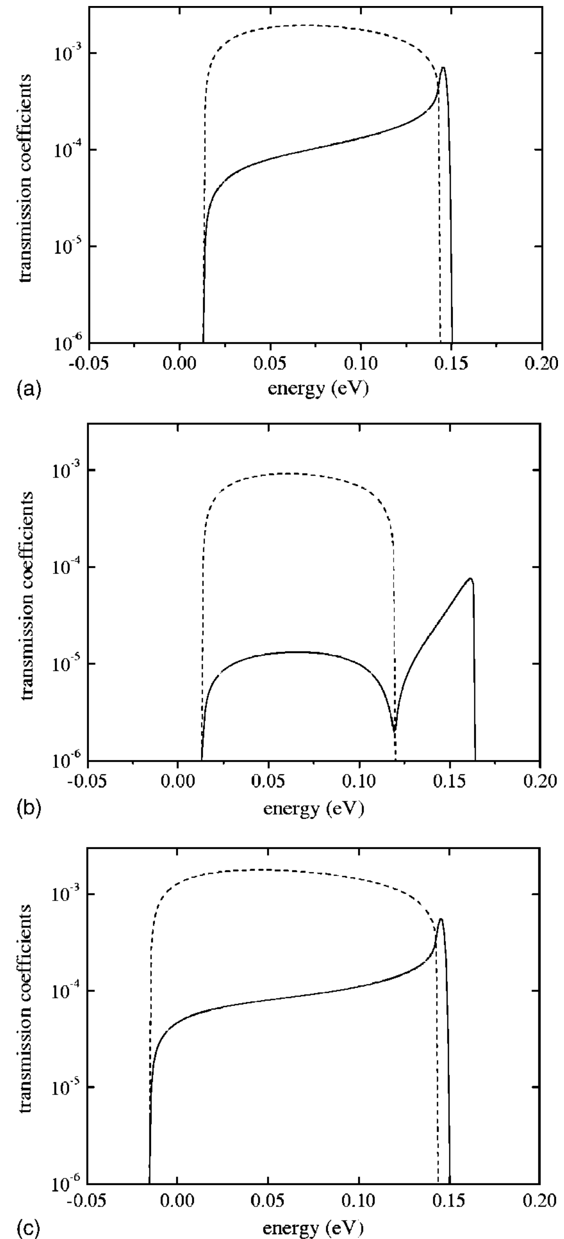

FIG. 2. The transmission coefficients for InAs/AlSb/GaSb structures under flatband conditions for the magnitude of the in-plane wave vector $k_{\parallel}=0.09\ \mathrm{nm}^{-1}$ (a) for the unstrained structure, (b) for the strained structure grown on InAs, and (c) for the strained structure grown on GaSb. The solid curves are for the CB-HH tunneling, and the dashed curves are for the CB-LH tunneling. The conduction-band edge of the unstrained InAs is used as the energy reference.

Figure 2 indicates that there is only one energy window for the CB-LH tunneling. The profiles of the transmission

[This article is copyrighted as indicated in the article. Reuse of AIP content is subject to the terms at: http://scitation.aip.org/termsconditions. Downloaded to] IP: 140.113.38.11 On: Thu, 01 May 2014 03:06:01

coefficient curves for the CB-LH tunneling in panels (a), (b), and (c) are qualitatively the same, except for the variation of the energy window width due to the energy-level change induced by strain. The left edges of the energy windows in panels (a) and (b) coincide, while that in panel (c) is essentially shifted to lower energies. This is because the conduction-band edge in the InAs layer is shifted downwards by 0.029 eV in the structure grown on GaSb. Therefore in this structure, for a given value of the electron in-plane wave vector in the InAs left contact layer, its component normal to interfaces becomes real at lower energy. Similarly, the redshift of the right edge of the energy window in panel (b) is due to the downward shift of the LH band edge in the strained GaSb right contact layer when the sample is grown on InAs. As a result, the normal component of the wave vector of the outgoing LH state in the GaSb layer vanishes at lower energy. We notice that the probabilities in panels (a) and (c) are larger than the probability in panel (b). The decrease of the CB-LH tunneling probability in panel (b) is due to the large downward shift of the LH valence-band edge in the strained AlSb barrier layer in a structure grown on InAs. This agrees with the experimental observation that the tunneling current density in samples grown on InAs is smaller than that in samples grown on GaSb.[4,5] We will return to this point later.

On the other hand, in panel (b) there are two energy windows for the CB-HH tunneling. The lower-energy window coincides with the energy window for the CB-LH tunneling. The higher-energy window, in which the CB-LH tunneling is forbidden, is created by the lattice-mismatch-induced strain. With strain decreasing, the lower-energy window expands toward the higher-energy side, while the higher-energy window shrinks. When the strain is absent in GaSb, the two energy windows merge into one, as shown in panels (a) and (c). The right edges of the energy windows for the CB-HH tunneling in panels (a) and (c) and of the second energy window in panel (b) correspond to the energies for which the normal component of the wave vector of the outgoing HH state in the GaSb cladding layer vanishes. The CB-HH tunneling probability is also weaker in panel (b) than in panels (a) and (c) for all energies, except for those which are near the right edge of the second energy window, resulting in a smaller current density in the structure grown on InAs.

For a given value of $k_\parallel$ the transmission coefficient depends on the direction of $\mathbf{k}_\parallel$ because of the anisotropy of the bulk dispersion of holes in various layers of the structure, resulting from the difference between Luttinger parameters ($\gamma_2 \neq \gamma_3$) and also from the lattice-mismatch-induced strain. This anisotropy of the transmission coefficients can be significant when the value of $k_\parallel$ is large. In the case of a small $k_\parallel$, it is much less than the absolute values of the normal to interfaces components of the wave vectors of the hole states in AlSb and GaSb for most energies, except for those close to the boundaries of energy windows for the CB-LH and CB-HH tunnelings. Then for real $k_{z,j}^{(n)}$, the angle between the wave vectors of states which have different directions of $\mathbf{k}_\parallel$ is small that results in negligible difference in bulk dispersion. Also, negligible difference in bulk dispersion can be found in

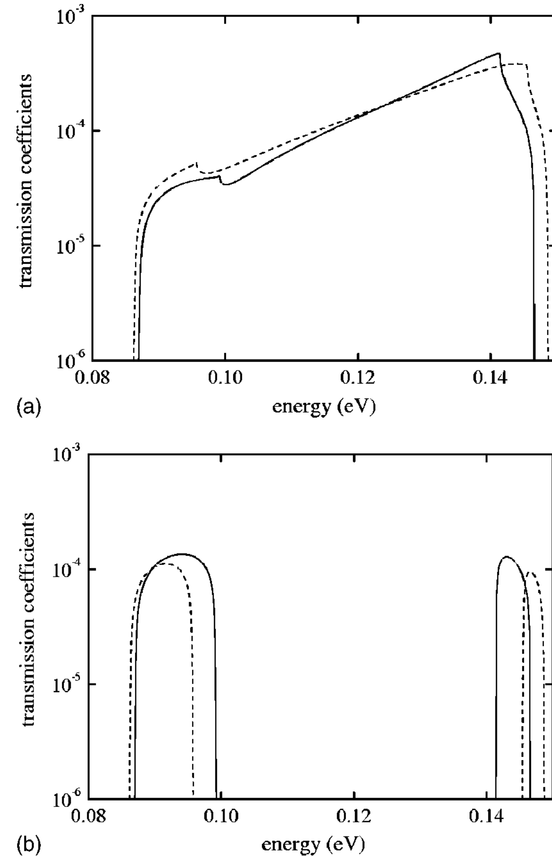

FIG. 3. The transmission coefficients for the InAs/AlSb/GaSb structure grown on InAs for the in-plane wave vector $\mathbf{k}_\parallel = 0.245\ \mathrm{nm}^{-1}$ (a) for the CB-HH tunneling and (b) for the CB-LH tunneling. The solid curves are for $\mathbf{k}_\parallel$ along the [10] direction, and the dashed curves are for $\mathbf{k}_\parallel$ along the [11] direction.

the case of complex $k_{z,j}^{(n)}$ if $|k_{z,j}^{(n)}| \gg k_\parallel$. For this reason the anisotropy of the transmission coefficients with respect to different directions of $\mathbf{k}_\parallel$ is also small. The anisotropy is enhanced with increasing $k_\parallel$, and to illustrate this phenomenon we have performed a detailed numerical study for $k_\parallel = 0.245\ \mathrm{nm}^{-1}$, at which the anisotropic effect is noticeable. The results are shown in Fig. 3 for an InAs/AlSb/GaSb sample grown on InAs, with panel (a) for the CB-HH tunneling and panel (b) for the CB-LH tunneling. The solid curves are for $\mathbf{k}_\parallel$ along the [10] direction and the dashed curves are for $\mathbf{k}_\parallel$ along the [11] direction. While the CB-HH tunneling probability is less anisotropic, profound anisotropic features are found in the CB-LH tunneling probability, the profile of which displays two separated narrow-energy windows.

Figure 4 shows similar results for an InAs/AlSb/GaSb sample grown on GaSb. Here again we see a weak anisotropy in the CB-HH transmission through the sample. However, for the CB-LH tunneling, an additional very narrow high-energy window appears in the transmission coefficient profile when $\mathbf{k}_\parallel$ switches from the [11] direction to the [10] direction. To find the origin of this additional sharp peak in the CB-LH tunneling probability, we performed another calculation for an unstrained structure using the axial approximation.[18] The results are shown in Fig. 5 with the solid curve for the CB-HH tunneling and the dashed curve

[This article is copyrighted as indicated in the article. Reuse of AIP content is subject to the terms at: http://scitation.aip.org/termsconditions. Downloaded to] IP: 140.113.38.11 On: Thu, 01 May 2014 03:06:01

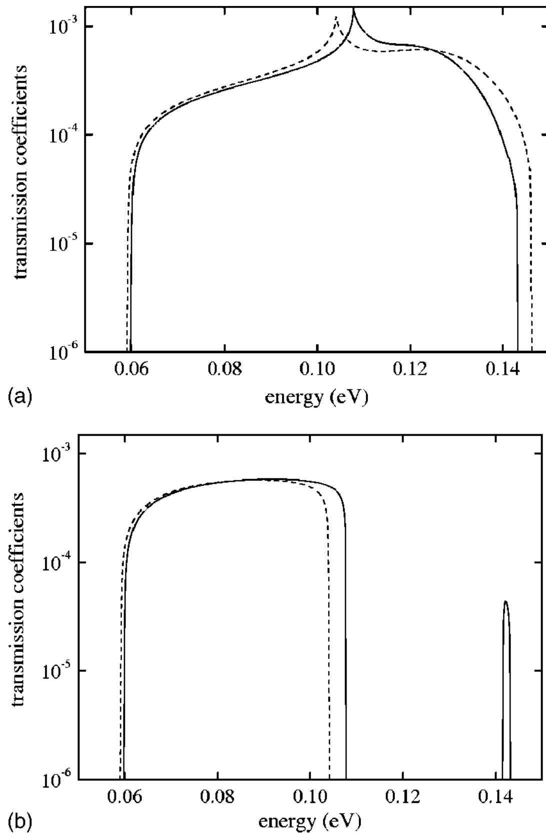

FIG. 4. The transmission coefficients for the InAs/AlSb/GaSb structure grown on GaSb for the in-plane wave vector $\mathbf{k}_{\parallel}=0.245\ \mathrm{nm}^{-1}$ (a) for the CB-HH tunneling and (b) for the CB-LH tunneling. The solid curves are for $\mathbf{k}_{\parallel}$ along the [10] direction, and the dashed curves are for $\mathbf{k}_{\parallel}$ along the [11] direction.

for the CB-LH tunneling. We see clearly in Fig. 5 the absence of the sharp peak in the high-energy regime. Consequently, this sharp peak is caused by the anisotropy of the hole spectrum in bulk GaSb which is generated by both the inequality of the Luttinger parameters $\gamma_2 \neq \gamma_3$ and the strain induced by the lattice mismatch. Because of the complicated anisotropic dispersion of holes in GaSb, at large values of $k_{\parallel}$ it is possible to have three different critical energies, at each of which k_z of the outgoing LH state in the GaSb cladding

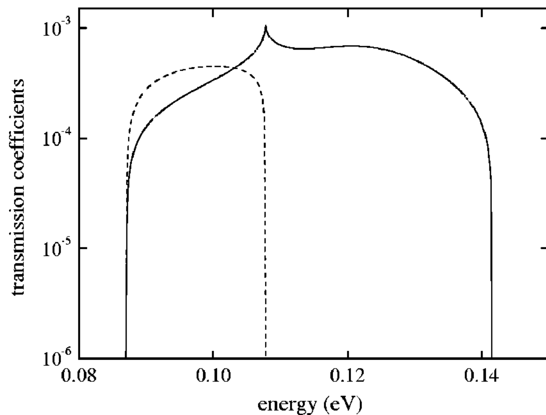

FIG. 5. The transmission coefficients for the unstrained InAs/AlSb/GaSb structure calculated with the axial approximation. The solid curve is for the CB-HH tunneling, and the dashed curve is for the CB-LH tunneling.

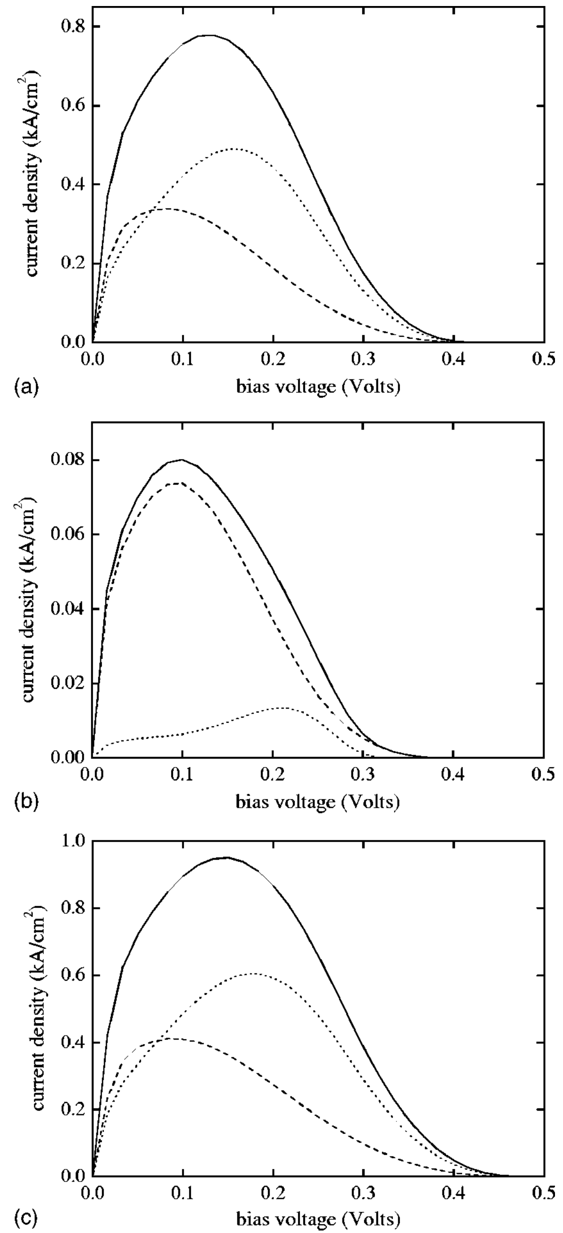

FIG. 6. The current–voltage characteristics of the InAs/AlSb/GaSb structures at the temperature of 77 K (a) for the unstrained structure, (b) for the strained structures grown on InAs, and (c) for the strained structures grown on GaSb. The solid curves are for the total current density, the dashed curves for the CB-HH contribution, and the dotted curves for the CB-LH contribution.

layer vanishes. These three critical energies correspond to the right edge of the lower-energy window for the CB-LH tunneling and the two edges of the higher-energy window. With further increase of $k_{\parallel}$ to $0.3\ \mathrm{nm}^{-1}$, the CB-LH tunneling and the CB-HH tunneling become forbidden.

Since we found that the anisotropy of the transmission coefficients is small for most of the tunneling processes, it cannot be detected in the $I-V$ characteristics. To calculate the $I-V$ curves, we have set the donor concentration in the left InAs cladding layer and the acceptor concentration in the right GaSb cladding layer to be $10^{17}\ \mathrm{cm}^{-3}$, which are the values for the experimental samples.[4] Our calculated $I-V$ curves at 77 K are shown in Fig. 6, where panel (a) is for an unstrained InAs/AlSb/GaSb structure, panel (b) is for a

[This article is copyrighted as indicated in the article. Reuse of AIP content is subject to the terms at: http://scitation.aip.org/termsconditions. Downloaded to] IP: 140.113.38.11 On: Thu, 01 May 2014 03:06:01

strained structure grown on InAs, and panel (c) is for a strained structure grown on GaSb. The solid curves are for the total current which consists of two components: the CB-HH tunneling contribution shown by the dashed curves and the CB-LH contribution indicated by the dotted curves.

Our finding of larger tunneling current densities in panels (a) and (c), as compared to that in panel (b), is consistent with the corresponding transmission coefficients in Fig. 2. Among the three cases in Fig. 6, only in panel (b) is the contribution of the CB-HH tunneling process larger than that of the CB-LH tunneling process for all the values of the applied voltage. In this sample, the HH band edge of GaSb lies above the LH band edge by approximately 0.048 eV. Hence holes occupy mainly the HH states in the GaSb cladding layer, and thus the tunneling into the HH states is the dominating process. Small hole occupation of the LH states in the GaSb cladding layer in the structure grown on InAs is another reason for the strong suppression of the CB-LH tunneling current component and the total current density in this sample. We would like to point out that in panel (b) when the CB-LH tunneling current vanishes at higher bias voltage, the CB-HH tunneling current density is still significant. This is due to the splitting of the GaSb valence band. At high voltages, the band edge for the light-holes becomes lower than the conduction-band edge of the InAs cladding layer near the barrier, and the tunneling into the LH states becomes forbidden.

We notice that the peak current density for the strained sample grown on GaSb is higher than that grown on InAs, in agreement with the experimental observations.[4,5] More precisely, the peak current density of about 0.95 kA/cm^2 in Fig. 6(c) is in good agreement with the experiment for the structure with a 3-nm barrier thickness.[4] (The observed value obtained from Fig. 4 in Ref. 4 is about 0.8 kA/cm^2.) The peak current density of about 0.08 kA/cm^2 in Fig. 6(b) is less than that in Ref. 5, which is about 0.16 kA/cm^2. This difference is due to the larger donor concentration in the InAs cladding layer and the acceptor concentration in the GaSb cladding layer (10^{18} cm^{-3} and 5×10^{18} cm^{-3}, respectively) of the experimental sample grown on InAs. Our calculation for the sample with these doping levels at room temperature, at which the experiments were performed in Ref. 5, gives an excellent agreement with the experiment for the peak current density.

B. Double-barrier structures

The tunneling current in the double-barrier InAs/AlSb/GaSb/InAs/AlSb/GaSb structure grown on GaSb was investigated experimentally in Ref. 9. In one of the experimental samples, in the quantum well the width of the GaSb layer is 6.5 nm and the width of the InAs layer is 12 nm. In our calculation, we use these layer widths. The energy-level structures in InAs/GaSb quantum wells were derived earlier,[19,26] and we have performed such calculations for the quantum well with 6.5-nm GaSb and 12-nm InAs and have used this information to assign the resonant-tunneling peaks obtained in our present work. The two barriers in the experimental sample have the same width of 3 nm, which produce very narrow widths of the resonant levels in the well. If we use this barrier width in our calculation, it will take an impractical amount of computer time to derive the $I-V$ curves. Hence, for practical purposes, we set the barrier width to 1.5 nm.

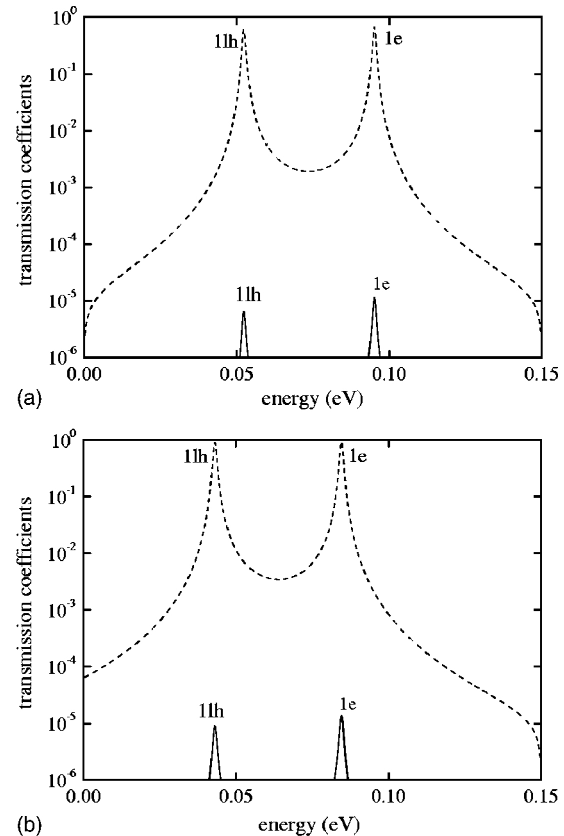

FIG. 7. Transmission coefficients for the InAs/AlSb/GaSb/InAs/AlSb/GaSb structure for small in-plane wave vector $\mathbf{k}_{\parallel}=0.001$ nm^{-1}. The solid curve is for the unstrained structure and the dashed curve is for the strained structure.

For CB-HH and CB-LH interband tunneling with in-plane wave vector $k_{\parallel}=0.001$ nm^{-1}, our calculated transmission coefficients are shown in Fig. 7, where panel (a) is for tunneling through an unstrained structure and panel (b) is for a strained one. The solid curves are for the CB-HH tunneling and the dashed curves are for the CB-LH tunneling. The labels $1e$ and $1lh$ indicate the resonant tunneling through the electronlike and the LH-like levels in the InAs/GaSb quantum well, while the interband tunneling through the HH-like states in the well is negligible for such a small value of $k_{\parallel}$. Also, the HH states are almost decoupled from the other states for $k_{\parallel}=0.001$ nm^{-1} and the transmission coefficients into the HH states are very small. We notice that both the $1e$ and $1lh$ states shift downwards due to the lattice-mismatched strain. The shift of the $1e$ level is due to the shift of the conduction-band edge in the strained InAs layer, while the shift of the $1lh$ level is most likely a result of its hybridization with the $1e$ level.

With a large value of the in-plane wave vector, an electron can also tunnel through the HH-like states. Because there is no inversion symmetry in the quantum well, the spin splitting of each energy level doubles the number of

[This article is copyrighted as indicated in the article. Reuse of AIP content is subject to the terms at: http://scitation.aip.org/termsconditions. Downloaded to] IP: 140.113.38.11 On: Thu, 01 May 2014 03:06:01

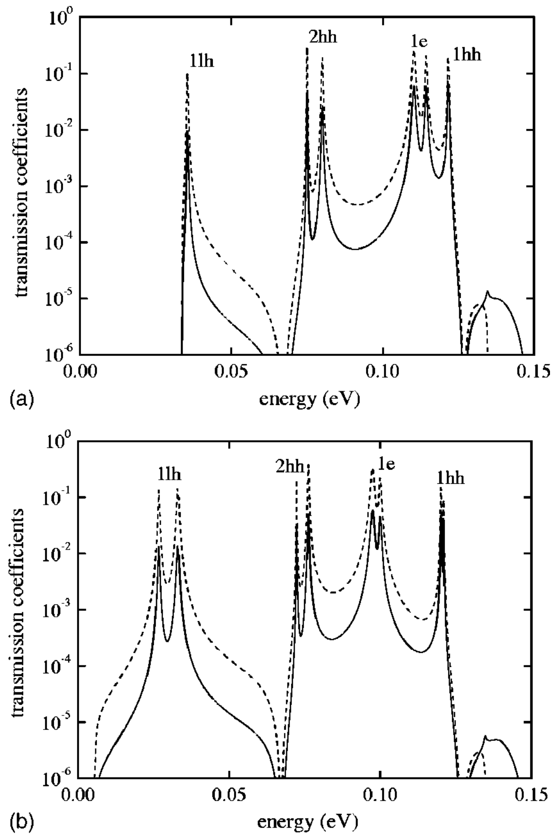

FIG. 8. The transmission coefficients for the InAs/AlSb/GaSb/InAs/AlSb/GaSb structure for in-plane wave vector $\mathbf{k}_{\|} = 0.145\ \mathrm{nm}^{-1}$ (a) for the unstrained structure and (b) for the strained structure. The solid curves are for the CB-HH tunneling, and the dashed curves are for the CB-LH tunneling.

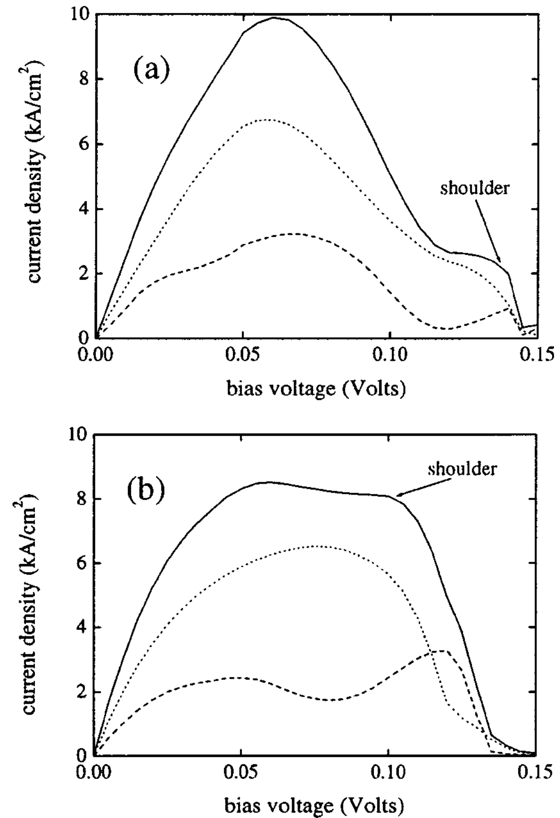

FIG. 9. The room-temperature (300 K) current–voltage characteristics of the InAs/AlSb/GaSb/–InAs/AlSb/GaSb structure (a) for the unstrained structure and (b) for the strained structure grown on GaSb. The solid curves are for the total current density, the dashed curves for the CB-HH contribution, and the dotted curves for the CB-LH contribution.

resonant-tunneling channels, resulting in the spin splitting of each peak of the transmission coefficient. For $k_{\|} = 0.145\ \mathrm{nm}^{-1}$, the calculated transmission coefficients are shown in Fig. 8. Since the anisotropy is negligibly small for such a magnitude of the in-plane wave vector, in Fig. 8 we only show the transmission coefficients for the $\mathbf{k}_{\|}$ along the [10] direction. The top panel (a) is for an unstrained sample, and the bottom panel (b) is for a strained one. The CB-HH tunneling is shown in solid curves and the CB-LH in dashed curves. The labels $1hh$ and $2hh$ indicate the tunneling through the first and second HH-like quasibound levels in the well. The strain-induced shifts of the $1hh$ and $2hh$ levels are small because of the weak coupling of these states to the $1e$ state.[26] The spin splitting exhibited in our sample is much larger than that reported for the InAs/GaSb/AlSb/GaSb structure.[11] The enhancement of the spin splitting here is due to the strong asymmetry of the structure. The spin splitting changes with the lattice-mismatched strain. We found the additional peak of the transmission coefficients caused by tunneling through the light-hole states in the quantum well for the strained sample. These processes become permitted because of the lowering of the conduction-band edge in the strained InAs cladding layer.

Using these transmission coefficients to calculate the tunneling current through the above studied InAs/AlSb/GaSb/InAs/AlSb/GaSb RTS, we need to specify the bipolar doping in both cladding layers. To be realistic, we set the donor concentration to be $10^{18}\ \mathrm{cm}^{-3}$ and the acceptor concentration to be $5 \times 10^{18}\ \mathrm{cm}^{-3}$, which are the doping levels in the experimental samples.[9] Our calculated $I-V$ characteristics at 300 K are shown in Fig. 9, where panel (a) is for the unstrained structure and panel (b) is for the strained one. The solid curves represent the total current density with the contributions from the CB-HH tunneling current in dashed curves and from the CB-LH tunneling current in dotted curves. The difference between the shapes of the two $I-V$ curves is consistent with the difference between the two transmission coefficient profiles in Fig. 8. Since the $1lh$ levels in the quantum well are much lower than the Fermi energy in the GaSb cladding layer for all positive bias voltages, the interband tunneling occurs mainly through the $1e$ and $2hh$ levels in the well and with little contribution from being through the $2hh$ levels. In an unstrained structure, the $1e$ level and $1hh$ level are closer to each other, and therefore may produce a sharper peak of the current density. The experimentally observed $I-V$ curve[9] has more shoulders as compared with the $I-V$ curve in Fig. 9(b). This may be explained by the fact that the barrier width of the experimental sample is 3 nm instead of the 1.5 nm used in our calculation.

IV. CONCLUSION

In summary, we have demonstrated that the bulk anisotropy and the strain induced by the lattice mismatch can have a significant influence on the interband tunneling processes

[This article is copyrighted as indicated in the article. Reuse of AIP content is subject to the terms at: http://scitation.aip.org/termsconditions. Downloaded to] IP: 140.113.38.11 On: Thu, 01 May 2014 03:06:01

in broken-gap heterostructures. We should mention that in our analysis, we have not considered the intraband processes, such as the thermionic emission processes and intraband tunneling of holes. These processes may affect the valley current density,[4,13,17] but will not change our results qualitatively. We should point out that the charge transfer from the GaSb layer to the InAs layer will modify the energy-level positions in the InAs/GaSb quantum well of the RTS. Assuming a reasonable amount of 2×10^{11} cm^{-2} for the transfer of electron concentration, from solving the Poisson equation we obtain an energy-level shift of only about 4 meV. Hence, a self-consistent calculation will not change our results qualitatively.

ACKNOWLEDGMENTS

This work was financially supported by the Russian Foundation for Basic Research (Grant No. N 03-02-16788), the Nordic Academy of Research Education, and the Swedish Foundation for International Cooperation in Research and Higher Education.

[1]J. R. Söderström, D. H. Chow, and T. C. McGill, Appl. Phys. Lett. **55**, 1094 (1989).
[2]L. F. Luo, R. Beresford, and W. I. Wang, Appl. Phys. Lett. **55**, 2023 (1989).
[3]D. Z.-Y. Ting, D. A. Collins, E. T. Yu, D. H. Chow, and T. C. McGill, Appl. Phys. Lett. **57**, 1257 (1990).
[4]R. Beresford, L. F. Luo, K. F. Longenbach, and W. I. Wang, Appl. Phys. Lett. **56**, 952 (1990).
[5]J. F. Chen, L. Yang, M. C. Wu, S. N. G. Chu, and A. Y. Cho, J. Appl. Phys. **68**, 3451 (1990).
[6]K. F. Longenbach, L. F. Luo, and W. I. Wang, Appl. Phys. Lett. **57**, 1554 (1990).
[7]E. E. Mendez, H. Ohno, L. Esaki, and W. I. Wang, Phys. Rev. B **43**, 5196 (1991).
[8]E. E. Mendez, Surf. Sci. **267**, 370 (1992).
[9]Y.-H. Wang, M. H. Liu, M. P. Houng, J. F. Chen, and A. Y. Cho, IEEE Trans. Electron Devices **41**, 1734 (1994).
[10]R. R. Marquardt, D. A. Collins, Y. X. Liu, D. Z.-Y. Ting, and T. C. McGill, Phys. Rev. B **53**, 13624 (1996).
[11]D. Z.-Y. Ting, E. T. Yu, and T. C. McGill, Phys. Rev. B **45**, 3583 (1992).
[12]M. S. Kiledjin, J. N. Schulman, K. L. Wang, and K. V. Rousseau, Phys. Rev. B **46**, 16012 (1992).
[13]M. A. Davidovich, E. V. Anda, C. Tejedor, and G. Platero, Phys. Rev. B **47**, 4475 (1993).
[14]Y. X. Liu, R. R. Marquardt, D. Z.-Y. Ting, and T. C. McGill, Phys. Rev. B **55**, 7073 (1997).
[15]J. Genoe, K. Fobelets, C. Van Hoof, and G. Borghs, Phys. Rev. B **52**, 14025 (1995).
[16]A. Zakharova and K. A. Chao, J. Phys.: Condens. Matter **14**, 5003 (2002).
[17]I. Lapushkin, A. Zakharova, V. Gergel, H. Goronkin, and S. Tehrani, J. Appl. Phys. **82**, 2421 (1997).
[18]A. Zakharova, Semicond. Sci. Technol. **13**, 569 (1998).
[19]A. Zakharova, S. T. Yen, and K. A. Chao, Phys. Rev. B **66**, 085312 (2002).
[20]D. Y. K. Ko and J. C. Inkson, Phys. Rev. B **38**, 9945 (1988).
[21]M. G. Burt, J. Phys.: Condens. Matter **4**, 6651 (1992).
[22]B. A. Foreman, Phys. Rev. B **56**, R12748 (1997).
[23]A. Zakharova, S. T. Yen, and K. A. Chao, Phys. Rev. B **69**, 115319 (2004).
[24]E. Halvorsen, Y. Galperin, and K. A. Chao, Phys. Rev. B **61**, 16743 (2000).
[25]M. P. C. M. Krijn, Semicond. Sci. Technol. **6**, 27 (1991).
[26]A. Zakharova, S. T. Yen, and K. A. Chao, Phys. Rev. B **64**, 235332 (2001).

[This article is copyrighted as indicated in the article. Reuse of AIP content is subject to the terms at: http://scitation.aip.org/termsconditions. Downloaded to] IP: 140.113.38.11 On: Thu, 01 May 2014 03:06:01